Bending fatigue of hybrid composite rods

N.K. Kar, , E. Barjasteh, Y. Hu, S.R. Nutt

Gill Composites Center, Department of Chemical Engineering and Materials Science, Vivian Hall of Engineering 402, University of Southern California, Los Angeles, CA 90089, United States

Abstract:

The flexural fatigue behavior of hybrid composite rods comprised of unidirectional carbon and glass fibers was investigated. Damage was evaluated by monitoring stiffness loss as a function of cycles, and bending fatigue failure was defined in terms of strength retention. The acoustic emission technique and microscopic examination were used to characterize damage progression and failure mechanisms. The number of cycles to failure depended on applied stress level, and a two-parameter Weibull analysis was used to incorporate probability of failure to the *S–N* curve. Damage initiated and propagated as a result of matrix cracking and fiber bundle failures within the GF shell. Bending fatigue damage only initiated when the hybrid was exposed to a deflection in excess of 42% of flexural strength, which does not occur in actual conductor field use. Damage reached a saturation point along the GF/CF interface because of the stress concentration that existed between the two material systems, resulting in asymptotic behavior of the stiffness loss. Because damage did not extend into the CF core, static mechanical properties were retained to ~85% or more.

Key words: A. Carbon fibers; A. Glass fibers; B. Fatigue; D. Acoustic emission homogenization

Membrane-type metamaterials: Transmission loss of multi-celled arrays
Naify, Christina J. and Chang, Chia-Ming and McKnight, Geoffrey and Scheulen, Florian and Nutt, Steven, Journal of Applied Physics, 109, 104902 (2011), DOI:http://dx.doi.org/10.1063/1.3583656

1. Introduction

Although polymer composites have been widely used in the aerospace industry for decades, the use of composites in other industries has been limited in part by the uncertainty in long-term durability [1]. However, this situation is changing, as evidence of the emergence of non-aerospace applications, such as electrical power transmission lines. Traditionally, overhead conductors feature conductive Al strands wrapped around a steel cable (termed ACSR, for aluminum conductor steel reinforced). The next generation of overhead conductors may involve replacement of the steel cable core in ACSR with a unidirectional hybrid (carbon/glass fiber) composite rod [2]. Composite-supported conductors (termed ACCC for aluminum conductor/composite core) will enable more economic and efficient transmission of electrical power [3]. Other advantages of the ACCC cables include greater strength, lower weight, and less sag at high temperatures then traditional steel-reinforced conductors.

The long-term durability of the ACCC conductor is an important issue, because overhead conductors are expected to operate maintenance-free and retain mechanical properties for decades. The effects of long-term exposure to heat and moisture on such hybrid composites were reported recently, and showed that the oxidized surface layer protected the bulk epoxy from further oxidation, and the complex intermingling of GF/CF interface acted as a temporary moisture barrier [4] and [5]. In general, the mechanical and physical properties of polymer composites are adversely affected by such environmental factors, and the ability to forecast changes in material properties as a function of environmental exposure is required to design for extended service life [6] and [7].

"Bending fatigue of hybrid composite rods" NK Kar, E Barjasteh, EJ Bosze, and SR Nutt, Compos A 42 [3] (2011) 328-336 DOI<http://dx.doi.org/10.1016/j.compositesa.2010.12.012>.

Overhead conductors typically experience crosswinds, which in certain conditions can result in galloping and Aeolian vibration, inducing dynamic tensile and flexural stresses [8]. Typically, Aeolian vibrations are high-frequency (>150 Hz) and cause small deflections. Nevertheless, such vibrations generate dynamic stresses that in some cases have caused fatigue failures in conventional transmission lines [8] and [9]. While composites are generally resistant to fatigue damage, recent highly publicized failures of carbon–fiber reinforced plastics (CFRP) have been partly attributed to fatigue [10] and [11].

An unresolved issue surrounding fatigue of composites is the predominant mechanism(s) responsible for fatigue failure. Some have concluded that local matrix failures are the primary mechanism involved, while others have suggested that gradual deterioration of the load-bearing fibers is primarily responsible [12] and [13]. Supporting the latter point of view, Agarwal et al. concluded that the dominating mechanism involved fiber failures, and that fatigue resistance was not strongly dependent on interface behavior [14]. Others have concluded that interfacial debonding is one of the most important life-limiting parameters in fatigue of composites [15].

In this paper, the bending fatigue behavior and failure mechanisms in unidirectional hybrid composite rods were investigated. The composite differs from most conventional composite laminates, and is a solid rod featuring a CF core and a GF shell. Flexural fatigue tests were performed, and phenomenological, log-normal, and Weibull models were employed to correlate fatigue life with stress level. The effect of bending fatigue on mechanical property retention was also investigated and analyzed.

2. Experiments

2.1 Materials

Unidirectional composite rods were produced by pultrusion (Composite Technology Corporation, Irvine, CA). The rods were comprised of a carbon fiber core (CF) surrounded by a glass fiber shell (GF), as described in [4] and [5]. The core consists of carbon fiber-reinforced epoxy, while the shell is comprised of glass fiber-reinforced epoxy. Fiber volume fractions and core/shell radii are indicated in Table 1. The epoxy matrix was designed to achieve a high glass transition temperature (T_g = 205 °C) using a propriety epoxy formulation and a curing agent.

Table 1.Hybrid composite properties.

	r_i(mm)	r_o(mm)	% Glass volume	% Carbon volume	% Epoxy volume	% Cross sectional area
CF-epoxy core	0	3.4	0	69	31	51
GF-epoxy shell	3.4	4.75	64	0	36	49

2.2 Mechanical and fatigue properties

The influence of flexural fatigue on mechanical properties was determined from measurements of post-fatigue flexural strength. Production composite rods 9.5 mm in diameter were cut to a length of 305 mm using a diamond saw, and flexural static tests were conducted on specimens using a three-point bend fixture to determine static flexural properties according to ASTM D790-2. A span ratio (L/d) of 20 was chosen for static and fatigue tests to minimize the effect of the shear stress and to maximize the effect of the flexural stress.

Fixed displacement, sinusoidal, flexural fatigue tests were performed at a frequency of 5 Hz using a load frame (Instron 8501) with a 100 kN load cell following ISO 13003. The displacement ratio Rd, which is the ratio of minimum displacement to the maximum displacement, was zero for all tests. Tests were conducted at five cyclic displacement levels (CDL), which corresponded to initial applied stress levels ranging from 47% to 68% of the flexural strength (FS). To monitor the degradation of mechanical properties, the dynamic stiffness was measured continuously as a function of the number of cycles (along with acoustic emission, described below). Tests were terminated when the cyclic stiffness was reduced by a percentage of the initial cyclic stiffness measured at each displacement.

Retained flexural strength and flexural modulus were determined after bending fatigue at each CDL. The effect of flexural fatigue on retained tensile strength (TS) of the composite core was measured according to ASTM Standard D3916 using a load frame (Instron 5585). Composite rods were mounted in the load frame using custom-made fixtures. The load was applied using a crosshead speed of 5 mm/min until failure occurred.

2.3 Finite element analysis

Finite element Analysis (FEA) was used to determine the stress distribution between the CF core and the GF shell during flexural loading. The specimen was modeled to represent the geometrical features of the test setup, using exact dimensions from the experiment. Load and boundary conditions were simulated with commercially available FEA software (ABAQUS and SolidWorks FEA Simulation Package) using 22,494 elements and C3D8R element type. A 3D model was implemented utilizing constituent properties of the GF shell and CF core specified by the manufacturer.

3. Monitoring damage development

3.1 Definition of damage and fatiguw failure

Global damage caused by fatigue in composites can be effectively monitored by measuring stiffness degradation [16]. A global damage index, *D* can be defined as:

$$D = \left(1 - \frac{(EI)_n}{(EI)_1}\right) \quad (1)$$

where $(EI)_n$ is the cyclic stiffness after the *n*th cycle, and $(EI)_1$ is the stiffness measured on the first cycle [17] at the tested CDL. The cyclic stiffness is different from the static flexural stiffness in that it is measured at the tested CDL, and not at the static failure displacement. The damage index *D*, is a measure of the degradation of the stiffness, and can be determined with techniques developed by previous investigators [17]. All individual damage mechanisms are assumed to contribute to this global damage parameter [18]. If a composite sample loses the ability to sustain stress before the point of separation, the definition of fatigue failure by catastrophic separation is of limited value. Therefore, fatigue failure is sometimes defined as the point in time when the composite can no longer sustain a specified stress level. Because of different processing techniques used to produce composites and the wide range of applications, these definitions are generally adapted to the loading environment.

Alternatively, fatigue failure of composites is often defined as the point when a global degradation percentage is reached, based on engineering justifications. For example, Kukureka et al. adopted a failure criterion of a 1.5% decrease in modulus because it caused a 10% reduction in flexural strength [19]. The most widely used criterion for fatigue failure is when the residual load bearing

capacity falls to the level of maximum stress in the fatigue cycle, at which point failure occurs [20]. However, this criterion can only be used for constant load fatigue tests, so different criteria have been adopted for constant displacement fatigue tests. For example, Shih et al. arbitrarily chose a 10% drop in load as fatigue failure for unidirectional fiberglass composites produced by matched mold fabrication [15]. One standard (ISO 13003) defines the end of a fatigue test as a damage level related to a specific reduction in specimen stiffness, generally between 5% and 20%.

In the present study, we defined fatigue failure in terms of the retained flexural strength after static loading. Quasi-static, three-point bend tests were performed to determine the maximum flexural stress (FS), σ_0. Once the composite failed at the static failure displacement (SFD), the load dropped sharply and the maximum stress was recorded. A surface crack caused by buckling on the GF compression surface was visible at the point of contact between the composite and fixture load pin, and cracks within the CF core were also visible. This buckling behavior dominates bending failure of composite beams because of the relatively low compressive strength of the fibers [21]. The composite was reloaded in a second three-point bend test to determine the residual maximum flexural strength σ. Once the composite failed a second time, the test was stopped. This procedure was performed on four samples to determine damage accumulated due to static flexural failure. The results shown in Table 2 indicate that after static flexural failure, the sample could support a stress that was roughly 80% of the FS. The flexural modulus could not be measured on reloading because the static tests became non-linear after initial failure. However, to approximate a similar amount of damage during flexural fatigue, a 20% drop in cyclic stiffness was chosen based on the assumption that during flexural fatigue, a relative drop in cyclic stiffness (at a fixed displacement) will cause the same percentage drop in both the static flexural modulus and static flexural strength.

Table 2. Retained stress and damage accumulation.

Test	Maximum flexure stress (MPa)	Retained strength (%)	Damage (%)
Initial stress	1033.46 ± 36.77	–	–
Retained stress	857.19 ± 7.38	82.9 ± 3.4	17.1 ± 3.4

3.2 Acoustic emission technique

The acoustic emission (AE) technique is a non-destructive method that has been used to determine the type of damage mechanisms occurring in composite fatigue. Any type of damage event occurring in a fiber-reinforced composite releases energy and produces a transient elastic wave [22]. Thus, direct information of fracture mechanisms can be determined from knowledge of the AE signals generated during loading. AE amplitude distributions have been used to identify damage mechanisms and monitor failure processes, where a rise in the frequency of AE events has been attributed to an increased level of damage in a material [23]. A single damage mechanism (such as matrix cracking) can produce a wide range of AE signal parameters, and overlap of parameter distributions can be caused by signal attenuation [24] Consequently, various amplitude ranges have been assigned for specific failure modes, and this practice is accepted within the context of a specified test setup [25]. To determine the dominant failure mechanisms during bending fatigue, the AE amplitude and number of events were plotted as a function of position and time.

Damage development was monitored during flexural fatigue tests using an acoustic emission system (Physical Acoustics PCI-2). Two 300 kHz resonance transducers (Micro 30) were placed on the loading fixtures to determine when and where damage events took place. The sensors were attached to model 2/4/6 preamps providing 40 dB of gain and band-pass filtering of 200–400 kHz. The location of the AE source in the specimen was determined using a linear location method. Only the events recorded between the sensors were used to analyze the AE results. A threshold level of 30 dB was used to filter out the interference caused by the hydraulics.

The most important AE parameters for burst-type signals are counts, amplitude, duration and absolute energy. Counts represent the number of times the signal amplitude crosses a set threshold level. Amplitude is the highest peak waveform voltage and is directly related to the type of event taking place within the material. Duration represents the time interval between the first threshold crossing and the last threshold crossing during an event, and absolute energy represents the area under the rectified signal envelope. A complexity associated with acoustic emission caused by fatigue arises from friction sources caused by the fretting of crack faces [26]. One approach to eliminating frictional sources involves varying AE parameters, although because both damage and friction events are largely stochastic, the corresponding AE signal parameters are also expected to overlap [27]. However Barre and Benzeggagh [23] showed that GF systems can exhibit signature AE amplitudes depending on the fracture mode, and produce both high and low amplitude events. Because both glass fibers and carbon fibers are present in this hybrid composite, failure mechanisms occurring in the GF shell and CF core should be distinguishable, because GF systems are more likely to emit high amplitude signals due to their larger size and failure strain.

4. Results and discussion

4.1 Flexural fatigue response

The typical flexural fatigue behavior of the hybrid composite is shown in Fig. 1, where damage growth is plotted as a function of the number of cycles (N) at various CDLs. As anticipated, increasing the displacement caused the number of cycles to failure (N_f) to decrease because of the higher stress exerted on the composite. Below 42% of FS, no stiffness loss occurred up to one million cycles and thus, a minimum stress was necessary to initiate damage.

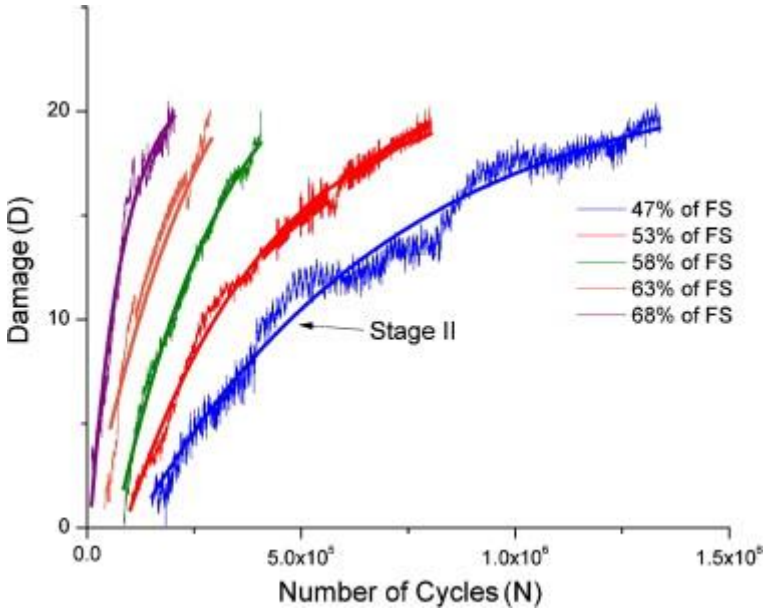

Fig. 1. Damage growth during Stage II fatigue at increasing stress levels.

The fatigue response is characterized by two stages. Stage I represents a "steady state" response in which no change in the damage variable was detected despite visible signs of degradation, while during Stage II, significant losses in the load-bearing capability of the composite occurred. In the figure, only Stage II is depicted because most of the damage took place during this stage. As the stress level increased, the number of cycles to initiate Stage II decreased. Larger displacements produced larger stresses in the composite, increasing the probability of initiating and propagating damage.

An analytical relationship was developed to relate damage to the number of cycles and applied stress level based on the damage saturation behavior shown in Fig. 1. This phenomenological approach provides a relationship between applied stress level and cycles to failure based on an interpretation of the observed phenomenon, although it does not take into account statistical scatter. The damage (D) can be expressed by:

$$D = A\ln(N) + C \qquad (2)$$

"Bending fatigue of hybrid composite rods" NK Kar, E Barjasteh, EJ Bosze, and SR Nutt, Compos A 42 [3] (2011) 328-336 DOI<http://dx.doi.org/10.1016/j.compositesa.2010.12.012>.

where *A* and *C* are material constants that depend on the applied stress level, and can be appropriately fit using regression analysis. Thus, for any stress level within the range that was tested, the number of cycles to failure can be expressed as:

$$N_f = \exp\left(\frac{D_f - C}{A}\right) \tag{3}$$

This expression is valid for the given CDL range during Stage II up to a damage index of 20%. Once the accumulated damage reaches 20% at any CDL, fatigue failure is assumed, and the test is complete.

The rate of damage accumulation during Stage II, (d*D*/d*N*) can be directly determined by numerical differentiation, and a power-law equation can be used to relate the rate of damage to the number of cycles, as shown below:

$$\frac{dD}{dN} = AN^B \tag{4}$$

Here, *A* and *B* are material constants, and *A* depends on the initial stress level, while *B*is the slope in Fig. 2. The damage rate decreases with increasing number of cycles, as shown in Fig. 2. The larger displacements correspond to more rapid initial damage rates because of the greater cyclic stresses applied. At all CDLs, the damage rates were greater during the initiation of Stage II, and decreased monotonically with increasing number of cycles as the composite approached failure. The monotonic decrease in damage rate was attributed to depletion of sites for damage development and a reduction of the stress gradient within the composite, both of which reduced the driving force to initiate and propagate damage [28]. When the stress was reduced, the increment of damage per cycle decreased. Ultimately, the composite approached a saturated damage state near the end of its fatigue

life, as shown in Fig. 1. The damage rate decreased with the number of cycles independently of CDL, indicating that the applied stress levels and the difference between strain rates within the range of tested displacements did not affect the deceleration of the damage rate.

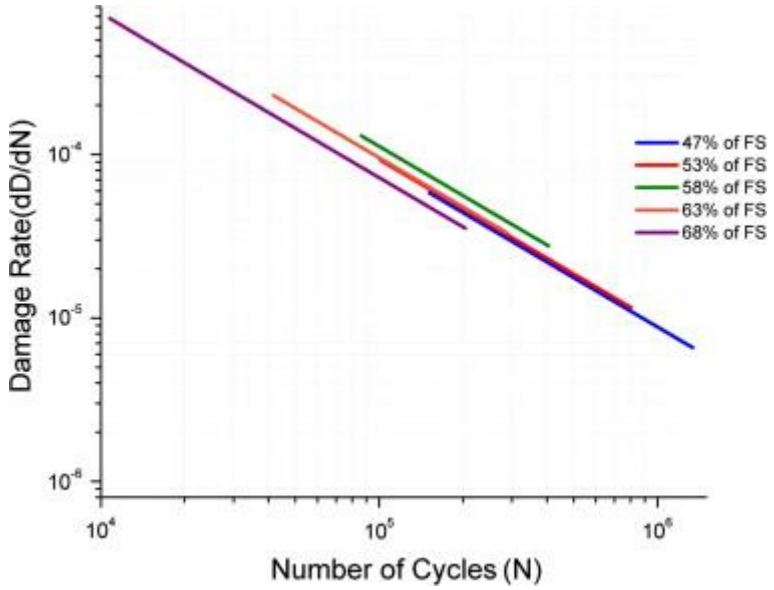

Fig. 2. Damage rate versus number of cycles at increasing stress levels.

4.2 Fatigue life under flexural loading

A log-linear relationship was developed between the number of cycles to failure and applied stress level (Wöhler curve), as shown in Eq. (5):

$$\log N_f = E + F\left(\frac{\sigma_1}{\sigma_s}\right) \tag{5}$$

where E and F are constants, σ_1 is the maximum cyclic stress on the first cycle, and $\sigma_s$is the FS. At least four samples were tested at each CDL to develop a comprehensive data set for the statistical model, and a 95% confidence band for the constant E was computed using statistical methods described in [29]. Fig. 3 shows the log-linear relationship and the associated confidence intervals. As the stress increased, the number of cycles to fatigue failure decreased in a log-linear fashion. The

scatter in fatigue life can be attributed to natural variability in the material properties, and to the anisotropic and inhomogeneous nature of the composite. The analytical model described previously provides a single life prediction for each tested stress level, while the log-normal model provides a more accurate prediction of fatigue life because it accounts for statistical scatter.

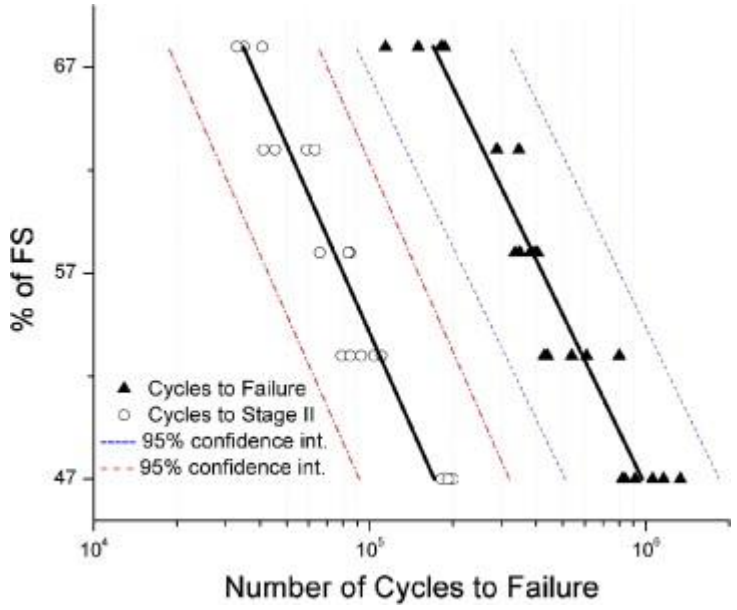

Fig. 3. S–N curve for flexural fatigue behavior of hybrid composite.

Fig. 3 also shows the number of cycles to initiate Stage II (N_{II}) as a function of CDL. The CDL had the same effect on N_{II} as on N_f, because the slopes for each linear regression were almost identical, as shown in Eqs. (6a) and (b):

$$\log N_{II} = 6.7823 - 0.033\left(\frac{\sigma_1}{\sigma_s}\right) \quad R^2 = 0.93 \tag{6a}$$

$$\log N_f = 7.681 - 0.0361\left(\frac{\sigma_1}{\sigma_s}\right) \quad R^2 = 0.91 \tag{6b}$$

Both N_{II} and the slope are useful indicators of the fatigue resistance of the material [10], and can help designers to predict fatigue behavior when changes in processing parameters and material

properties are introduced. The Wöhler curve can be used as a method for life prediction and is one way to present statistical data, although it does not incorporate probability of failure into the *S*–*N* relationship. Instead, it indicates to designers that 95% of the time, the composite will fail within the specified interval.

An alternative to the log-normal assumption is a two-parameter Weibull analysis, which provides a way of computing failure probabilities so that designers can compare the reliability of different designs or estimate the fatigue life at a given stress level for a desired probability of failure. In this investigation, the cumulative distribution function (CDF), *F(x)* was used to incorporate such a relationship, as shown below:

$$F(x) = 1 - e^{-\left(\frac{x}{\alpha}\right)^{\beta}} \tag{7}$$

in which x is the specific value of the random variable (N_f), α is the scale parameter or characteristic life at the specified CDL, and β is the shape parameter. The scale and shape parameters were determined at each CDL using Bernard's Median Rank (*MR*) formula:

$$MR = \frac{i - 0.3}{k + 0.4} \tag{8}$$

where i is the failure order number and k is the total number of samples tested at the CDL [30]. A plot was constructed of $\ln(\ln(1/1 - MR))$ versus $\ln(N_f)$, and a linear regression fit was used to determine the Weibull parameters for the specified stress level (not shown). The correlation coefficient for the linear regression fits was ~0.90 or greater, indicating the suitability of Weibull analysis for the present study. The values for α and β obtained for each CDL are shown in Table 3.

Using these values and incorporating selected failure probabilities (F_p) fatigue life was predicted according to the relation below:

$$N_f = \exp\left(\frac{\ln\left[\ln\left(\frac{1}{1-F_p}\right)\right] + \beta \ln \alpha}{\beta}\right) \quad (9)$$

where the number of cycles at which the median population of the composites fail for a given stress level could be determined [30]. The predicted fatigue lives of the hybrid composite population at failure probabilities ranging from 25% to 95% are shown in Fig. 4. The plot shows that the number of cycles to failure, N_f, declined with increasing stress level in log-linear fashion, which is consistent with Fig. 3. The plot shows the percentage of the composite rod population that will fail at a given stress level, as well as the distribution of predicted N_f values.

Table 3. Weibull parameters at various stress levels.

% of FS applied	Scale parameter (α)	Shape parameter (β)
47	1023447.06	6.53
53	543191.82	5.58
58	385437.46	13.74
63	309447.41	2.57
68	172992.79	4.33

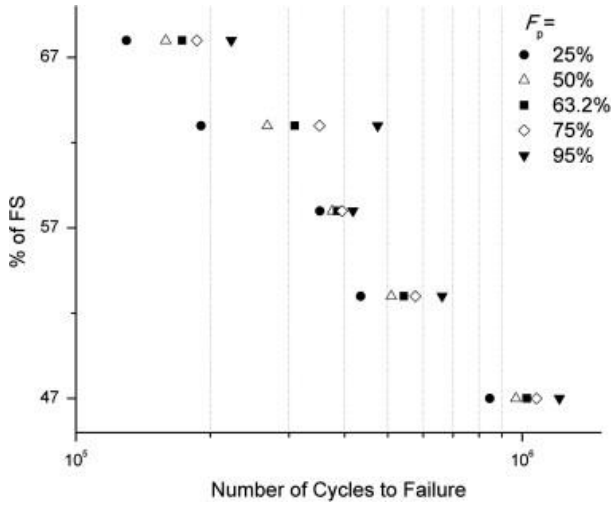

Fig. 4. S–N curve utilizing failure probabilities.

The three methods used to determine fatigue life relied on different approaches and provided different insights. The phenomenological approach quantitatively described how damage accumulates with number of cycles, but provided only a single prediction for each CDL. In contrast, the Wöhler curve provided a way to present the set of fatigue data and assumed that scatter was independent of applied stress level, where fatigue life was log-normally distributed. Although this log-normal distribution function has been used extensively in fatigue analysis, Gumbel showed that with the log-normal distribution, the probability of failure after surviving a given number of cycles decreased with increasing time [31]. This assertion is not valid when applied to degradation of engineering materials, and he argued that there is no physical interpretation of the log-normal distribution for fatigue life. The third method, in which a two-parameter Weibull distribution was used to predict fatigue life at a specified probability of failure, provides designers a way to predict life with a certain level of confidence. To determine how well the Weibull model fit the set of observations, the Kolmogorov–Smirnov (K–S) goodness of fit test was used as follows:

$$D_i = \max_{i=1}^{k} \left(\left| \frac{i}{k} - F(x_i) \right| \right) \tag{1}$$

where $F(x_i)$ is the cumulative distribution in Eq. (9) and x_i is the cycles to failure for the$i$th test. The maximum value of D_i for each CDL was compared to D_c values obtained from a K–S table, and all values of D_i were less than D_c at a 5% level of significance, as shown in Table 4. Thus, the two-parameter Weibull CDF was appropriate to predict fatigue life and incorporated failure probabilities into the predicted *S*–*N* curve.

Table 4. Goodness of fit parameters.

% of FS applied	D_i	D_c
47	0.22	0.57
53	0.23	0.62
58	0.2	0.49
63	0.31	0.62
68	0.25	0.62

4.3 Failure mechanisms

Damage initiation and accumulation during flexural fatigue occurred in two stages, and the asymptotic growth in the damage variable (during Stage II) occurred in the same fashion at all CDLs. Fig. 5 shows the damage progression and AE events as a function of fatigue life for a specimen loaded at 68% of the FS. Both Stages I and II are shown and damage initiated in the GF shell at the midpoint of the sample on the tensile surface where the bending moment was greatest. The rise in AE activity between 8% and 17% of life was attributed to matrix cracking.

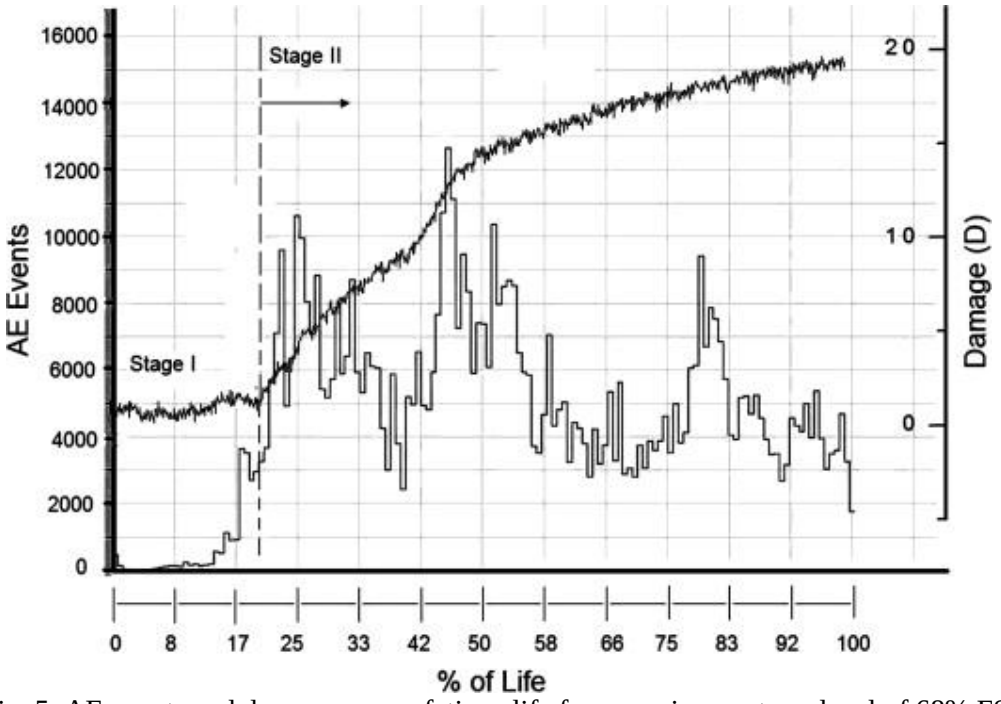

Fig. 5. AE events and damage versus fatigue life for a maximum stress level of 68% FS.

Initial damage sites during Stage I appeared as light surface patches, and closer SEM inspection revealed the development of matrix cracks, as shown in Fig. 6a. The limited cracking along the fiber/matrix interface indicated strong interfacial bonding, while matrix cracks extended in transverse directions (radial and circumferential) normal to the axial fibers. The interaction of such cracks resulted in a macroscopic brush-like appearance on the tensile surface, at the outermost region of the glass fiber shell. The brush-like appearance was caused by fiber fracture and the linkage of individual damage zones, which caused the detachment of fiber bundles from the glass shell, as shown in Fig. 6b. The formation of broken fiber bundles was accompanied by a sharp rise in the number of AE events near 17% life (see Fig. 5), and an increase in the damage variable, indicating the start of Stage II.

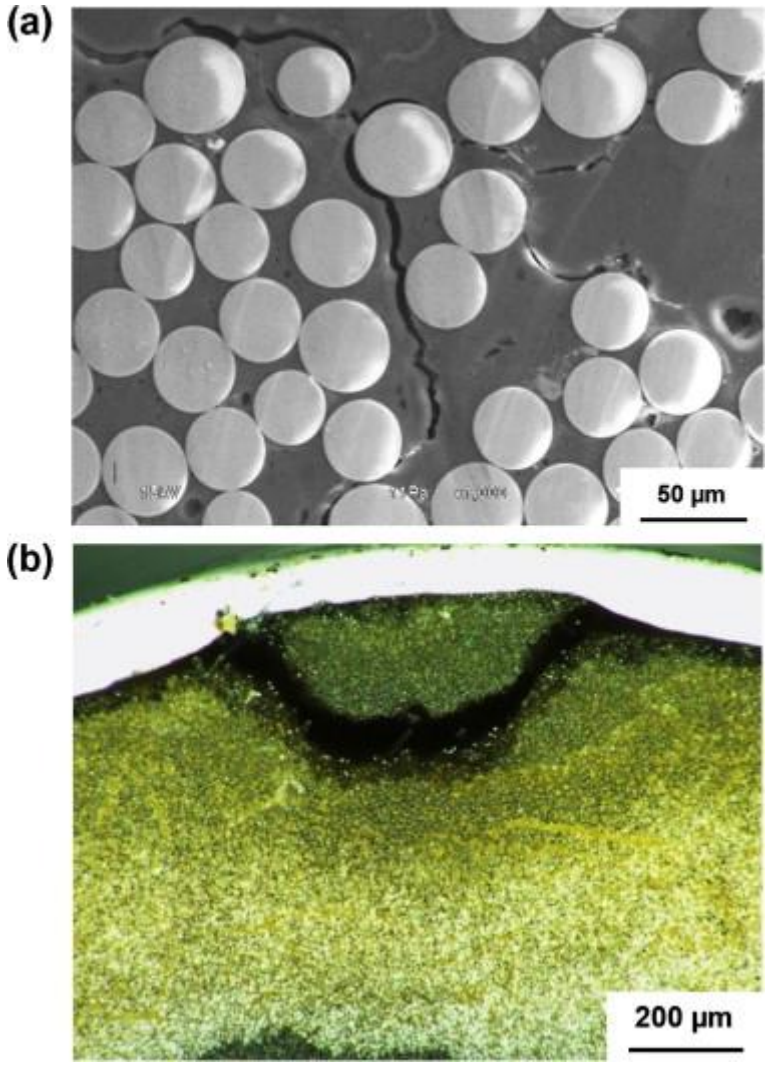

Fig. 6. (a), Damage initiates as transverse matrix cracks in the GF shell, (b) brush-like feature formation at top surface of shell.

Fig. 7 shows the AE amplitude distribution as a function of both position (along the specimen length) and life during Stages I and II. Between the start of the test and ~8% of fatigue life, a reduction in AE was observed, which can be attributed to the felicity effect (FE). The felicity effect is a phenomenon in which AE activity decreases (from unloading and reloading) because AE from initial sources end, and AE activity during reloading resumes at a fraction of the previously applied load [32]. AE activity resumed when the first fatigue mechanism was activated, marking the onset

of Stage I damage (indicated on figure). This initial damage source exhibited an amplitude range of 40–50 dB and was identified as matrix cracking. The start of Stage II is distinguished by the green[1] and red amplitude distribution in the center of the composite, ranging between 60 and 70 dB. These high-amplitude events correspond to multiple fiber bundle failures, where packets of GFs fail and could also be caused by continued matrix decohesion and cracking. Between fiber bundle failures, there were periods of activity in which only matrix cracking occurred. These periods occurred at ~33% of total life and again at ~66% total life (absence of green/red, indicated by red ellipses). During these periods, longitudinal splitting extended towards the specimen ends, creating crack surfaces normal to the load axis, while matrix cracking simultaneously propagated in transverse directions towards the neutral axis. Previous investigators have shown that friction caused by the fretting of crack faces can produce AE [33], and others have suggested that friction sources are of short duration, resulting in low-energy AE counts [19]. Thus, while frictional sources are present and produce AE counts, they account for only a minor portion of the AE data displayed.

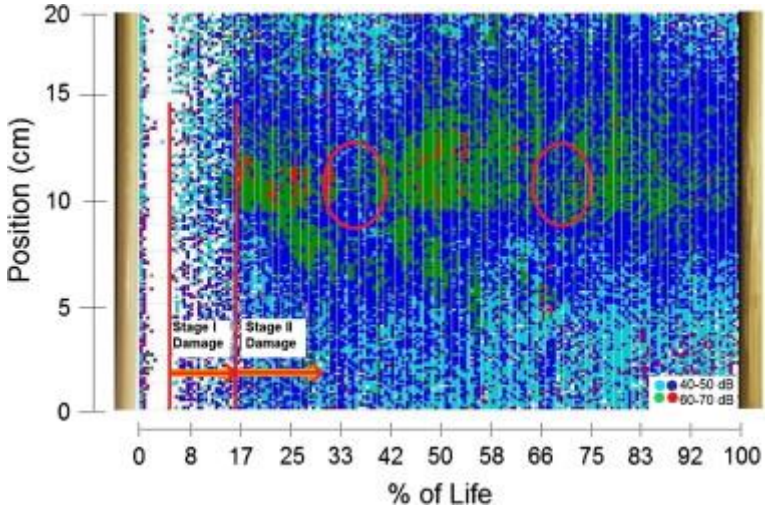

Fig. 7. AE amplitude distribution as a function of position and life.

"Bending fatigue of hybrid composite rods" NK Kar, E Barjasteh, EJ Bosze, and SR Nutt, Compos A 42 [3] (2011) 328-336 DOI<http://dx.doi.org/10.1016/j.compositesa.2010.12.012>.

Initial GF bundle breaks and attendant matrix cracking caused a redistribution of stress within the specimen. Matrix cracking effectively isolated certain fibers from load transfer, causing load shedding to proximal fibers, which contributed to additional fiber failures [34]. As Stage II proceeded, multiple fiber bundles failed, causing a continuous redistribution of stress. Matrix cracks propagated in longitudinal (horizontal) and radial directions, forming layer-like slabs that extended primarily in parallel planes normal to the loading direction. These parallel layers were joined by shorter radial crack segments that extended toward the CF/GF interface, as shown in Fig. 8. The "slab cracks" were a consequence of fiber bundle breaks that first occurred near the rod surface. Additional matrix cracks subsequently developed on roughly parallel planes successively deeper beneath the surface, creating additional slabs, and stopping at the GF/CF interface (see Fig. 8). The continuous loss in stiffness was attributed not to such matrix cracks, but to the fracture of multiple fiber bundles in the GF shell. Both fatigue mechanisms (matrix cracks and fiber bundle fractures) occurred concurrently during Stage II, and were interactive, in that transverse matrix cracking led to the formation of multiple fiber bundle failures, and vice versa. Fig. 7 shows that most of the high-amplitude events (indicated by red dots) took place early in Stage II and contributed to the majority of damage growth and the highest damage rate (as shown in Fig. 5). Near the end of the composite life, the number of AE events decreased, indicating a deceleration in damage rate and a subsequent saturation of damage along the interface. These phenomena are consistent with trends shown previously in Fig. 1 and Fig. 2.

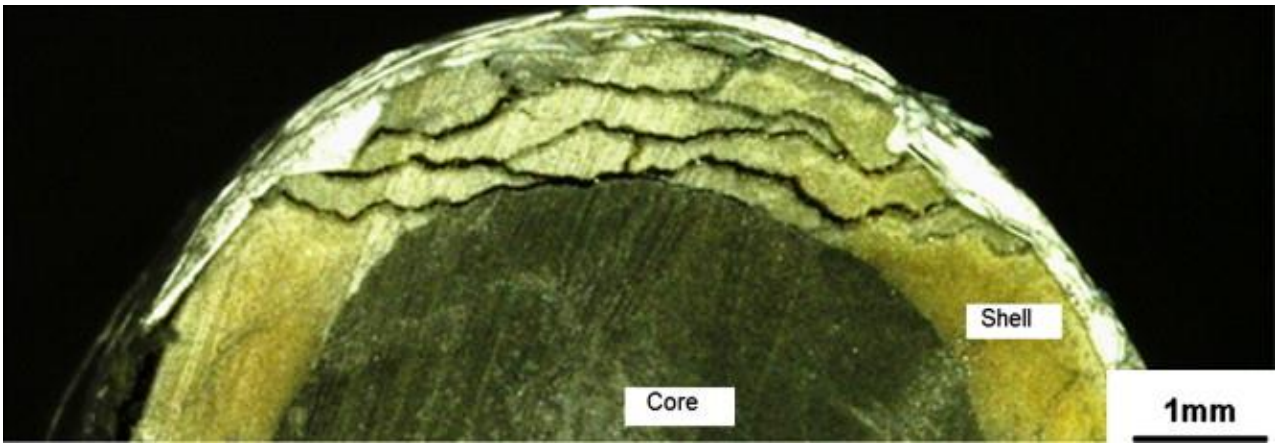

Fig. 8. Damage saturation at end of fatigue life.

"Bending fatigue of hybrid composite rods" NK Kar, E Barjasteh, EJ Bosze, and SR Nutt, Compos A 42 [3] (2011) 328-336 DOI<http://dx.doi.org/10.1016/j.compositesa.2010.12.012>.

4.4 Stress distribution along the CF/GF interface

During flexural fatigue, the maximum bending moment (M_c) occurred at the center of the specimen, and was distributed to the GF and CF regions. Although the maximum strain occurred at the outer surface of the GF shell, the maximum stress arose at the CF/GF interface because of the higher modulus of the CF/epoxy system. The axial stress (σ_a), within the GF shell or CF core can be calculated as follows:

$$\sigma_a = \frac{E_{GF/CF} r}{\rho} \tag{11}$$

$$\rho = \frac{E_{GF} I_{GF} + E_{CF} I_{CF}}{M_c} \tag{12}$$

where ρ is the radius of curvature, E_{GF} and E_{CF} are the moduli of the respective fiber–matrix systems, I is the second moment of inertia, and r is the distance from the neutral axis. The value of E depends on the system for which the stress is to be calculated. The axial stress distribution due to bending is shown in Fig. 9 for a specimen loaded to 68% of the FS.

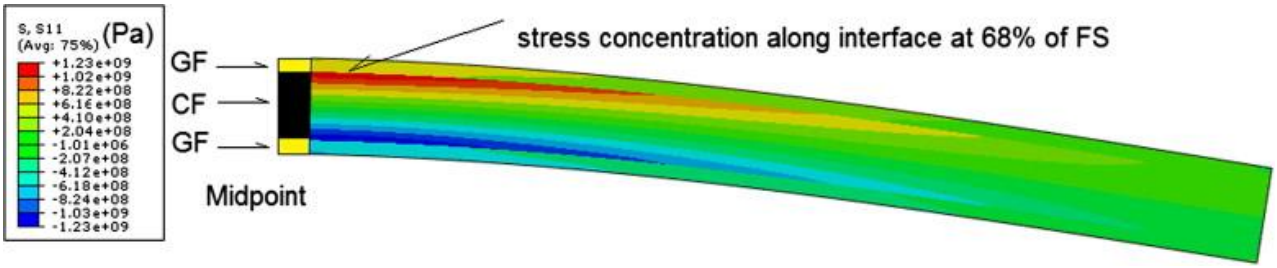

Fig. 9. FEA showing stress concentration along GF/CF interface.

The maximum axial stress, σ_a, occurs at the midpoint of the composite, and decreases linearly towards the sample ends, as expected. The axial stress at the midpoint varies with radial position, and is greatest at the CF/GF interface (see Midpoint in Fig. 9); where there is an abrupt discontinuity of stress that affects the way damage propagates during fatigue.

Fatigue damage first appeared in the form of matrix cracks followed by fiber bundle breaks in the GF shell. Once cracks reached the GF/CF interface, they stopped and did not penetrate into the CF core. The stress concentration at the interface caused cracks to propagate along this plane of maximum tensile stress, causing the observed asymptotic behavior in the damage variable (Fig. 5). Because cracks failed to penetrate the CF core, the progressive reduction in stiffness ceased. And while the interfacial portion of the CF system experienced the greatest cyclic axial stress (1.2 GPa), the ultimate tensile strength of the CF material (~3.4 GPa) prevented fatigue failure. Note that carbon fiber composites typically exhibit greater resistance to fatigue when compared to comparable GF composites [35].

The radial distribution of strain during cyclic loading affected the matrix stress within the GF and CF regions. During initial cyclic loading, the stress within the matrix at the outer surface of the GF shell was greater than the matrix stress along the interface in the CF core. The axial elastic stress within the matrix (σ_m) for each material system is given by:

$$\sigma m - CF = (Em)\varepsilon CF \quad (13)$$

$$\sigma m - GF = (Em)\varepsilon GF \quad (14)$$

where ε_{CF} is the maximum strain in the CF system, ε_{GF} is the maximum strain in the GF system and E_m is the elastic modulus of the matrix. The elastic strain is calculated by:

$$\varepsilon = \frac{r}{\rho} \tag{15}$$

Table 5 shows the respective stresses in the matrix at the tested stress levels. During Stage I, the surface strain produced a larger axial matrix stress at the surface than along the interface, causing the observed initiation of surface matrix cracks (and not along the interface). The maximum matrix stress in the CF system at the CF/GF interface was 26 MPa, which was nearly the same minimum matrix stress at the outer surface of the GF shell, indicating that a minimum stress in the matrix was necessary to initiate fatigue damage at any point within the composite.

Table 5. Stress within the matrix.

FS (%)	Curvature (*m*)	$\sigma_{m-GF}^{\max}$ (MPa)	$\sigma_{m-CF}^{\max}$ (MPa)
47	0.67	25	18
53	0.59	29	20
58	0.54	32	22
63	0.50	35	24
68	0.46	37	26

The development of matrix cracks is dependent on the modulus and strain-to-failure of the fibers [32]. The carbon fibers, because of their proximity to the neutral axis, experienced lower strains than the glass fibers. The CF modulus was also 3× greater than that of the GF modulus. These two factors limited the overall strain of the carbon core, limiting matrix deformation which might initiate fatigue mechanisms. Effectively, the GF shell acted as a protective buffer, preventing large strains in the carbon core. The GF shell was exposed to the largest strain, and because of the lower stiffness relative to the carbon fiber core, the working strains during fatigue led to matrix damage.

4.5 Retained mechanical properties

The retained flexural strength (FS) and flexural modulus (FM) were determined after fatigue failure occurred at each CDL. Fig. 10 shows that as the initial applied stress level increased, the retained FS and FM decreased. Specimens cycled at larger displacements were expected to retain less strength and stiffness, as higher stress levels caused more damage. The extent to which larger displacements caused more damage was evaluated by measuring retained properties. (Differences in damage from samples cycled at the various stress levels were not visibly discernable.) The retained FS and FM dropped concurrently during cyclic loading, although both properties showed 85–90% retention of original values. Note however that a 20% drop in cyclic stiffness during fatigue did not cause a 20% drop in static flexural modulus or flexural strength. The difference arises because the cyclic stiffness is measured at the specified CDL, and not at the SFD, and thus provides a measure of the relative stiffness. The extent of damage to the hybrid composite was a function of the CDL. Thus, the quasi-static flexural tests (discussed in Section 3.1) were more destructive to the hybrid composite than flexural fatigue tests (20% reduction in FS compared to 15%), because damage was introduced both to the GF surface and to the CF core (not shown) at the static failure displacement.

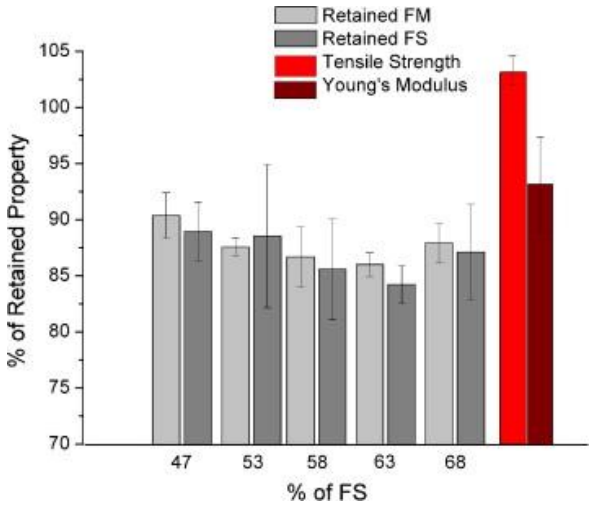

"Bending fatigue of hybrid composite rods" NK Kar, E Barjasteh, EJ Bosze, and SR Nutt, Compos A 42 [3] (2011) 328-336 DOI<http://dx.doi.org/10.1016/j.compositesa.2010.12.012>.

Fig. 10. Retained mechanical properties after flexural fatigue.

After fatigue loading at 63% of the FS, samples were mounted in tensile fixtures and uniaxial properties were measured. No loss in tensile strength of the hybrid composite rods was observed after fatigue failure. A synergistic effect does not exist for this composite, [3] and thus catastrophic failure occurred in tension as the hybrid reached the failure strain of the carbon fibers (2.1%). Because the GF shell carried ~25% of the applied tensile load and reached ~66% of its TS at failure, the maximum strength was not utilized under tensile loads. The primary purpose of the GF shell is to prevent galvanic coupling between the CF core and conducting aluminum wires. Thus, fatigue damage to the GF shell will only affect the TS of the hybrid composite if the strength of the GF shell declines by more than ~33%, or if fatigue damage propagated into the CF core, neither of which was observed in this study.

5. Conclusion

The flexural fatigue behavior of a GF/CF composite rod was investigated, and damage development was monitored to predict fatigue life at specified stress levels. Fatigue life was characterized by two distinct stages. Damage initiated by the formation of microscopic transverse matrix cracks on the GF tensile surface during Stage I. AE measurements revealed that during Stage II, both fiber bundle failures and matrix crack propagation played an interactive role in the progression of damage and reduction in stiffness. A distinctive failure pattern was observed, as radial and circumferential cracks made up layer like formations that saturated along the CF/GF interface.

"Bending fatigue of hybrid composite rods" NK Kar, E Barjasteh, EJ Bosze, and SR Nutt, Compos A 42 [3] (2011) 328-336 DOI<http://dx.doi.org/10.1016/j.compositesa.2010.12.012>.

An issue of practical importance concerns the effect of fatigue on long-term durability and retention of mechanical properties. Nearly 85–90% of the flexural strength and modulus were retained and no loss in tensile strength was observed. The flexural fatigue damage was limited to the glass fiber shell, and did not penetrate into the carbon fiber core. The GF shell effectively acted as a sacrificial barrier to fatigue, protecting the CF core from damage.

Note that when supporting overhead conductors in actual service conditions, the composite core will experience cyclic deflections from wind loading and aeolian vibration, but such deflections will be much smaller than those used in the present investigation. Aeolian vibration tests (IEEE 1138) and American Electric Power sequential test protocols were recently conducted on the ACCC conductor and showed no evidence of fatigue failure up to 100 million cycles. Nevertheless, the rods will be exposed to various cyclic stresses (axial and bending) over long periods and large numbers of cycles. Thus, it is important to understand fundamental fatigue damage mechanisms, the conditions necessary to activate them, and the associated effects on property retention and product lifetime. The hybrid composite design provides an effective means of limiting fatigue damage and delaying the onset of fatigue failure, both of which serve to promote long-term durability of composites used in infrastructure applications.

Acknowledgements: Financial support from Composite Technology Corporation is gratefully acknowledged. The authors also acknowledge Dr. Byungmin Ahn, Dr. Shad Thomas, Michael Asfaw and Dr. Ron Miller for their advice and support.

References:

1. K. Liao, C.R. Schultheisz, D.L. Hunston, **Long-term environmental fatigue of pultruded glass–fiber-reinforced composites under flexural loading,** Int J Fatigue, 21 (5) (1999), pp. 485–495
2. A. Alawar, E.J. Bosze, S.R. Nutt, **A composite core conductor for low sag at high temperatures,** IEEE Trans Power Deliv, 20 (3) (2005), pp. 2193–2199

"Bending fatigue of hybrid composite rods" NK Kar, E Barjasteh, EJ Bosze, and SR Nutt, Compos A 42 [3] (2011) 328-336 DOI<http://dx.doi.org/10.1016/j.compositesa.2010.12.012>.

3. E.J. Bosze, A. Alawar, O. Bertschger, Y.I. Tsai, S.R. Nutt, **High-temperature strength and storage modulus in unidirectional hybrid composites,** Comp Sci Tech, 66 (13) (2006), pp. 1963–1969
4. Y.I. Tsai, E.J. Bosze, E. Barjasteh, S.R. Nutt, **Influence of Hygrothermal environment on thermal and mechanical properties of carbon fiber/fiber glass composites,** Comp Sci Technol, 69 (3–4) (2009), pp. 432–437
5. E. Barjasteh, E.J. Bosze, S.R. Nutt, **Thermal aging of fiberglass/carbon–fiber hybrid composites,** Composites A, 40 (12) (2009), pp. 2038–2045
6. R. Selzer, K. Friedrich, **Mechanical properties and failure behavior of carbon fibre-reinforced polymer composites under the influence of moisture,** Composites A, 28 (6) (1997), pp. 595–604
7. F. Ellyin, R. Master, **Environmental effects on the mechanical properties of glass–fiber epoxy composite tubular specimens,** Comp Sci Technol, 64 (12) (2004), pp. 1863–1874
8. IEEE guide for aeolian vibration field measurement of overhead conductors. IEEE Std 1368; 2006. p. 1–35.
9. Whapham R, Champa RJ. Wind induced vibrations of overhead shield wires. In: Pacific coast electrical association engineering and operating conference, CA; 1983.
10. C. Bathias, **An engineering point of view about fatigue of polymer matrix composite materials,** Int J Fatigue, 28 (10) (2006), pp. 1094–1099
11. B. Harris, **Fatigue in composites,** CRC Press (2003) p. 4–5
12. Dharan CKH. Fatigue failure in fiber-reinforced materials. In: Proceedings of ICCM-1 conference; 1975. p. 830–9.
13. M. Salvia, L. Fiore, P. Fournier, L. Vincent, **Flexural fatigue of UDGFRP experimental approach,** Int J Fatigue, 19 (3) (1997), pp. 253–262
14. B.D. Agarwal, L.J. Broutman, **Analysis and performance of fiber composites,** John Wiley and Sons, Inc., New York (1980)
15. G.C. Shih, L.J. Ebert, **The effect of the fiber/matrix interface on the flexural fatigue performance of unidirectional fiberglass composites,** Comp Sci Technol, 28 (2) (1987), pp. 137–161
16. B. Harris, **Fatigue and accumulation of damage in reinforced plastics,** Composites, 8 (4) (1977), pp. 214–220
17. M.H. Allah, E.M. Abdin, A.I. Selmy, U.A. Khashaba, **Short communication: effect of mean stress on fatigue behaviour of GFRP pultruded rod composites,** Composites A, 28 (1) (1997), pp. 87–91
18. A. Poursartip, M.F. Ashby, P.W.R. Beaumont, **The fatigue damage mechanisms of a carbon fibre composite laminate: development of the model,** Comp Sci Technol, 25 (3) (1986), pp. 193–218
19. S.N. Kukureka, C.Y. Wei, **Damage development in pultruded composites for optical telecommunications cables under tensile and flexural fatigue,** Comp Sci Technol, 63 (12) (2003), pp. 1795–1804
20. B.Y. Liu, L.B. Lessard, **Fatigue and damage-tolerance analysis of composite laminates: stiffness loss, damage-modelling, and life prediction,** Comp Sci Technol, 51 (1) (1994), pp. 43–51
21. G. Marom, H. Harel, S. Neumann, K. Friedrich, K. Schulte, H.D. Wagner, **Fatigue behaviour and rate-dependent properties of aramid fibre/carbon fibre hybrid composites, Composites, 20 (6) (1989), pp. 537–544**
22. Unpublished data from PCI-2 based AE system user's manual. Mistras group.
23. S. Barre, M.L. Benzeggagh, **On the use of acoustic emission to investigate damage mechanisms in glass–fibre reinforced polypropylene,** Comp Sci Technol, 52 (1994), pp. 369–376
24. W.H. Prosser, K.E. Jackson, S. Kellas, B.T. Smith, J. Mackeon, A. Friedman, **Advanced waveform-based acoustic emission detection of matrix cracking in composites,** Mater Eval (1995), pp. 1052–1058
25. I.M. De Rosa, C. Santulli, F. Sarasini, **Acoustic emission for monitoring the mechanical behaviour of natural fibre composites: a literature review,** Composites: Part A (2009), pp. 1456–1469

"Bending fatigue of hybrid composite rods" NK Kar, E Barjasteh, EJ Bosze, and SR Nutt, Compos A 42 [3] (2011) 328-336 DOI<http://dx.doi.org/10.1016/j.compositesa.2010.12.012>.

26. J. Awerbuch, M.R. Gorman, M. Madhukar, **Monitoring acoustic emission during quasi-static loading–unloading cycles of filament wound graphite epoxy laminate coupons,** Mater Eval, 43 (1985), p. 754
27. Y.A. Dzenis, **Cycle based analysis of damage and failure in advanced composites under fatigue 1. Experimental observation of damage development within loading cycles,** Int J Fatigue, 25 (2003), pp. 499–510
28. S.S. Wang, E.S.M. Chim, **Fatigue damage and degradation in random short-fiber SMC composite,** J Comp Mater, 17 (2) (1983), pp. 114–134
29. ASTM E 739-91. Standard practice for statistical analysis of linear or linearized stress-life (S–N) and strain-life (ε–N) fatigue data. ASTM international, West Conshohocken, PA; 2004.
30. R. Bedi, R. Chandra, **Fatigue-life distributions and failure probability for glass–fiber reinforced polymeric composites,** Comp Sci Technol, 69 (9) (2009), pp. 1381–1387
31. E.J. Gumbel, **Parameters in the distribution of fatigue life,** J Eng Mech (1963), pp. 45–63 ASCE
32. I.M. De Rosa, C. Santulli, F. Sarasini, **Acoustic emission for monitoring the mechanical behaviour of natural fibre composites: a literature review,** Composites A, 40 (9) (2009), pp. 1456–1469
33. J. Awerbuch, S. Ghaffari, **Monitoring progression of matrix splitting during fatigue loading through acoustic emission in notched unidirectional graphite/epoxy composite,** J Reinf Plast Comp, 7 (3) (1988), pp. 245–264
34. F.L. Matthews, G.A.O. Davies, D. Hitchings, C. Soutis, **Finite element modeling of composite materials and structures,** Woodhead Publishing, Berlin (2000) p. 198
35. J.F. Mandell, F.J. McGarry, J.Y. Hsieh, C.G. Li, **Tensile fatigue of glass fibers and composites with conventional surface compressed fibers,** Poly Comp, 6 (3) (1985), pp. 168–174

"Bending fatigue of hybrid composite rods" NK Kar, E Barjasteh, EJ Bosze, and SR Nutt, Compos A 42 [3] (2011) 328-336 DOI<http://dx.doi.org/10.1016/j.compositesa.2010.12.012>.